CARBON 58 (2013) 139–150

Available at www.sciencedirect.com

SciVerse ScienceDirect

journal homepage: www.elsevier.com/locate/carbon

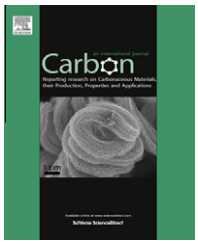

Graphene as catalyst support: The influences of carbon additives and catalyst preparation methods on the performance of PEM fuel cells

Angela Marinkas [a], *Francesco Arena* [a], *Jens Mitzel* [a], *Günther M. Prinz* [b], *Angelika Heinzel* [c], *Volker Peinecke* [c], *Harald Natter* [a,*]

[a] *Saarland University, Physical Chemistry, Campus Geb. B2 2, D-66123 Saarbrücken, Germany*
[b] *University Duisburg-Essen, Experimental Physics and CENIDE, Lotharstraße 1, D-47057 Duisburg, Germany*
[c] *ZBT Duisburg, The Fuel Cell Research Center GmbH, Carl-Benz-Str. 201, D-47057 Duisburg, Germany*

ARTICLE INFO

Article history:
Received 17 November 2012
Accepted 19 February 2013
Available online 27 February 2013

ABSTRACT

The reduction of the platinum amount for efficient PEM (polymer electrolyte membrane) fuel cells was achieved by the use of graphene/carbon composites as catalyst support. The influences of the carbon support type and also of the catalyst preparation method on the fuel cell performance were investigated with electrochemical, spectroscopic and microscopic techniques. Using pure graphene supports the final catalyst layer consists of a dense and well orientated roof tile structure which causes strong mass transport limitations for fuels and products. Thus the catalysts efficiency and finally the fuel cell performance were reduced. The addition of different carbon additives like carbon black particles or multi-walled carbon nanotubes (MWCNT) destroys this structure and forms a porous layer which is very efficient for the mass transport. The network structure of the catalyst layer and therefore the performance depends on the amount and on the morphology of the carbon additives. Due to optimizing these parameters the platinum amount could be reduced by 37% compared to a commercial standard system.

1. Introduction

Graphene is known as monolayers of sp^2 bonded carbon atoms into a two-dimensional structure and has become of rapidly expanding interest due to its extraordinary features such as high electronic and thermal conductivity [1,2,4], an ambipolar field-effect [3], intriguing (magneto-)transport characteristics [5,7], and mechanical properties [6]. Graphene exhibits also a very high surface area (~2630 $m^2 g^{-1}$) [8], much higher than graphite (~10 $m^2 g^{-1}$) or carbon nanotubes (1300 $m^2 g^{-1}$). All these remarkable properties make graphene promising for applications like polymer-composite materials [9], photo-electronics [10], field-effect transistors [11], electro-mechanical systems [12], sensors [13,15,16], hydrogen storage [14], energy conversion and storage, batteries [17] and drug delivery systems [18].

PEM fuel cells are clean and environmentally-friendly power sources, which are essential for future energy solutions [19]. They exhibit good energy efficiency and high power density per volume, but the high costs of the noble metal catalysts, electrolyte membranes, bipolar plates and the control system constrain a widespread commercialization. The MEA-fabrication costs (membrane electrode assemblies) can be reduced through several approaches such as (i) reducing the platinum loading (ii) the use of high temperature-tolerant membranes and (iii) new alternative electrocatalyst materials

* *Corresponding author:* Fax: +49 681 302 4759.
E-mail address: h.natter@mx.uni-saarland.de (H. Natter).
0008-6223/$ - see front matter
http://dx.doi.org/10.1016/j.carbon.2013.02.043

[20,21]. In the last 3 years some very promising efforts were made in electrode development and in membrane technology to reduce the price of fuel cell systems. Zirfon™ was sucsessfully tested to replace the expensive Nafion™-membranes [22] and activated carbon air-cathodes have a great potential as inexpensive alternative to Pt-catalysed electrodes in microbial fuel cells [23,24]. For electrochemical cogeneration of chemicals and also for NO/hydrogen fuel cells some effective concepts for the preparation of gas diffusion electrodes in a cold rolling or casting process with carbonaceous compounds and binders were reported recently [25].

Our strategy to lower the MEA-costs is the improvement of the cell performance by developing more efficient catalyst support systems which has the following properties:

(i) high specific surface area, which improves the dispersion of the catalytic metals,
(ii) improved chemical and electrochemical stability at operation temperatures between 60 and 100 °C,
(iii) enhanced electronic conductivity due to strong percolation, and
(iv) high catalytic activity for hydrogen oxidation of the graphene itself [26,27].

Currently, the most common electrocatalysts are platinum and platinum-based alloys supported on carbon black. A major problem of the catalysts is aggregation on the surface of the carbon black support [28]. A further problem is the formation of inactive catalysts during the manufacturing process that means about 30% of catalysts are not located at the triple-phase boundaries (TPBs) where the fuel cell reactions take place.

To reduce the amount of inactive catalysts, catalyst supports and also catalyst particles with a strong reduced size were developed [26] but these systems are very hard to handle in coating processes and additionally the very small catalyst particles are thermally instable. A third problem is the electronic conductivity because in such small carbon particles the graphite content is very low. Graphitized carbon black particles with good electronic conductivity have a larger specific surface of about 65 $m^2 g^{-1}$ (e.g. TIMREX™ HSAG400, Ensaco™ 350G). An alternative to conventional carbon black materials could be graphene flakes. The theoretical specific surface area of single-layer graphene is about 2600 $m^2 g^{-1}$, but the specific surface area of multilayer graphene is much smaller (70–130 $m^2 g^{-1}$). An advantage of these materials is the high graphite content. Only a few fundamental research results for the preparation of isolated metal particles on the surface of single-, double-, and few-layer graphene sheets [29,30] are known.

In addition to the active surface area of the catalyst/carbon black system, the stability is very important. There are two mechanisms of degradation: coalescence sintering and Ostwald ripening [27]. Coalescence sintering is enhanced by carbon corrosion which occurs under a high potential in an acidic environment. During the oxidizing process surface-oxygen containing species are formed and the catalyst–carbon interactions are weakened. Graphene may improve catalyst stability by providing a more stable support material and by strengthening the interaction of the catalyst with the support [26]. These enhanced interactions between the metal particles and the graphene surface are described in [31].

Finally, in a high-performance PEM fuel cell electrode the supported catalysts should be located at the TPBs. The flake-like structure of the graphene should lead to a very porous and percolated system which is essential for the mass transport and the electronic conductivity [32]. This work shows two routes of platinum catalyst immobilization on the surface of multilayer graphene flakes: (i) thermally-induced chemical reduction of a platinum precursor and (ii) electrochemical reduction of a platinum precursor by potentiostatic electrodeposition using a hydrogen depolarized anode (HDA).

The advantage of the first method is the decrease of the degree of agglomeration of platinum precursors during the reduction process because of the high interaction between adsorbed precursor ions and the graphene surface. The catalyst loading can be controlled by the amount of hexachloroplatinic acid. The HDA-method [33] has the advantage that it enables a very precise control of the catalyst loading and leads to a very homogeneous platinum particle distribution. This method assures the formation of nearly 100% of active catalyst particles which are located at the TPBs. The samples were characterized by ICP-OES, SEM, TEM, XRD and Raman spectroscopy. The electrodes were used to prepare MEAs which were characterized in a modular fuel cell test station.

2. Experimental

2.1. Materials

Many preparation methods for graphene and graphene oxide exist in the literature but most of them work in small laboratory scale [34–37]. The evaluation of graphene as catalyst support requires relatively large sample amounts in the range of 10–20 g, each. This amount can only be prepared in several batches in a time consuming and extensive way. For reproducibility reasons commercial graphene samples which are available in the required amounts were used (Table 1).

2.2. Microscopic techniques

TEM pictures (transmission electron microscopy) were taken with a JSM 6400 F instrument (Jeol, Munich, Germany). Samples were suspended with ethanol and applied on a TEM grid. SEM pictures (scanning electron microscopy) were taken using a Jeol JXA-840A microscope and Helios NanoLab™ 600

Table 1 – Properties of used commercial graphene samples purchased from Graphene Supermarket (Calverton, New York).

Graphene	BET Surface/$m^2 g^{-1}$	Average flake thickness	Average flake diameter
AO-2	100*	52 layers–13 nm	5.3–8.0 μm
C1	60*	32 layers–4 nm	5–23 μm

* Values taken from the manufacturer.

(FEI, Eindhoven, Netherlands). The samples were fixed in the dry, powdery state on the sample holders.

The AFM pictures (atomic force microscopy) were taken with a Nanoscope IV (Imstar, Paris, France). Graphene dispersions in N-methyl-pyrrolidone were applied on a silicon wafer. After drying the samples AFM measurements were performed to determine the structure after the coating process. The measured area of the sample was $15 \times 15\ \mu m^2$.

2.3. Raman spectroscopy

Raman spectroscopy measurements were performed using a custom-built μ-Raman setup. The setup consists of a Nd:VO_4 laser operating at 532 nm as excitation source, a microscope objective, a spectrometer, and a liquid nitrogen-cooled CCD camera. The diameter of the laser spot on the sample surface is about 1 μm (Laser powers: 100–350 μW). The light was spectrally analyzed using a 500 mm spectrometer, which is equipped with a 150 mm^{-1} grating and an attached CCD-camera. The spectra are recorded using backscattering geometry at room temperature. Two different types of graphene samples were investigated. For these measurements the graphene powders were first deposited on a SiO_2/Si-wafer. Then a second wafer was placed on top and the two wafers were rubbed against each other. Afterwards, the multilayer graphene flakes and their agglomerates were measured lying on the surface of the two SiO_2/Si-wafers. Pt-loaded flakes were also studied for the AO-2 sample as described in Section 3.2. The spectra were normalized and shifted for better clarity.

2.4. Chemical characterization

Chemical impurities were determined by optical emission spectroscopy (ICP-OES) measured with a Varian 720-ES (Varian Inc., Palo Alto, California). The samples were weighed and reduced to ashes in a three-step process: 120 min at 180 °C, 360 min heated up to 800 °C and finally 60 min at 800 °C, the residue was boiled in 28 mL nitrohydrochloric acid at 120 °C for 4 h. The resulting refluxed solution for analysis was obtained after the addition of HNO_3 (1 wt.%) to a volume of 100 mL. The results are listed in Table 3. The same procedure was also used to analyze the platinum contents of the catalyst layers.

2.5. Zeta potential analysis

The catalysts on the graphene surface were prepared by thermal/electrochemical reduction of surface adsorbed platinum precursors. For this reason the knowledge of the graphene surface potential is essential because the amount and the strength of the adsorption of platinum species depends on it. The Zeta potential of aqueous dispersions of pure AO-2 and C1 was measured at pH 7 with a Zetasizer (Malvern Instruments, Herrenberg, Germany).

2.6. Area specific electric resistance

The electronic conductivity of the catalyst support is important for the resulting performance of the complete MEA because the produced electrons are transported through the carbon supports to the current collectors. For this reason the area specific electric resistance of the graphene flakes was determined. First of all, an uncoated GDS (gas diffusion system) type H2315 I3 C4 from Freudenberg (Weinheim, Germany) was measured. All experiments were carried out in ex situ mode, meaning in the dry state and not in an operating fuel cell. The through-plane resistances of the coatings are very low compared to the total resistance, which will be dominated by the GDS. For this reason the area specific resistance has to be measured ex-situ because the small changes in the data cannot be resolved in an in-situ measurement which shows typical cell resistances in the range of 150 $m\Omega\ cm^2$. The sensor electrodes made of gold coated steel (area = 4 cm^2) were contacted directly to the GDS or to coated GDS samples. The mechanical pressures between the electrodes can be linearly controlled by air pressure in the compression piston system. The mechanical pressure was varied between 3 and 30 bar. The experiment was carried out 10 times for each sample. The accuracy of the experimental setup is ±1 $m\Omega\ cm^2$.

In a first experiment the pressure-dependent area specific resistance of an uncoated GDS was analyzed (Fig. 11). The resistance decreased from 27 $m\Omega\ cm^2$ at 2.5 bar to 17 $m\Omega\ cm^2$ at 30 bar, which can be explained with a lower transition (incl. contact) resistance for higher compacting pressure. In a second experiment the area specific resistance of two coated GDS samples were analyzed: one GDS sample was coated with a 10 μm thick Vulcan XC72R/Nafion™ layer and the second GDS sample was coated with a 10 μm thick layer consisting of graphene and Nafion™. The thickness of 10 μm corresponds to the thickness of catalyst layers with a platinum loading of 0.36 $mg\ cm^{-2}$ (40 wt.% Pt/C) used for further experiments.

2.7. Preparation of graphene dispersions

The preparation of graphene dispersions is often related to the graphene production, where the product is an aqueous dispersion which contains exfoliated graphene sheets [42]. Stable dispersions of graphene nanosheets can be prepared in organic solvents [43] and also in water. The literature reports about graphene dispersions with DMF (dimethylformamide), NMP (N-methyl-pyrrolidone), THF (tetrahydrofuran) or EG (ethylene glycol).

Different preparation methods for dispersions were tested:

(1) *Dispersion in isopropanol/water:* a mixture of 150 mg graphene, 1000 mg water and 1000 mg isopropanol (purchased by Sigma-Aldrich, Munich, Germany) were homogenized by ultrasonication for 10 min.
(2) *Dispersion in water/organic solvents:* 150 mg graphene, 1 mL water, 1 mL ethylene glycol and 5 mL isopropanol were ultrasonicated for 15 min. To enhance the dispersibility 150 mg 10 wt.% NaOH was added to the mixture (until pH = 10).
(3) *Dispersion in N-methyl-pyrrolidone:* 10 mg graphene was dispersed in 10 mL N-methyl-pyrrolidone (purchased by Sigma–Aldrich, Munich, Germany) and ultrasonicated for 10 min.

The stability of the resulting dispersions was evaluated after 24 h. Best results were obtained with AO-2 graphene in N-methyl-pyrrolidone or in isopropanol/water.

2.8. Chemical preparation of graphene-supported Pt catalysts

The graphene-, graphene/carbon black- or graphene/MWCNT-supported Pt catalysts (anode 19 wt.% Pt) were prepared by thermally-induced chemical reduction using a mixture of 35 mg H_2PtCl_6 (Umicore, Hanau, Germany, 40 wt.% Pt), 90 mg graphene, 10 mL water and 40 mL EG (purchased by Sigma-Aldrich). Hexachloroplatinic acid was dissolved in 10 mL H_2O. This solution was added under vigorous stirring to an aqueous suspension of 90 mg AO-2 graphene in 40 mL ethylene glycol. The mixture was heated at 120 °C for 24 h. The resulting product was washed with ethanol (purchased by Sigma-Aldrich) and centrifuged (Rotina 420, Hettich, Tuttlingen, Germany, 5000 rpm). The residue was dried for 12 h in vacuum.

The catalyst ink with a higher loading of 54 wt.% Pt was prepared under the same conditions, but with increased amounts of H_2PtCl_6 and graphene. The resulting powder, which contains Pt/graphene, Pt/graphene/carbon black or Pt/graphene/MWCNT, was first analyzed with optical emission spectroscopy to determine its exact platinum content. After that 375 mg graphene/carbon black or graphene/MWCNT supported catalysts were dispersed with 1 mL water, 1.28 mL isopropanol and 1.785 mL Nafion™ solution (20 wt.%) and ultrasonicated for 10 min until a homogenous dispersion was formed. The resulted catalyst ink was used to coat a $10 \times 20\ cm^2$ GDS by the doctor blade method using a 180 μm doctor blade (Erichsen, Hemer, Germany). The doctor blade was moved with a velocity of $5\ mm\ s^{-1}$. The resulted GDE was dried at 140 °C for 30 min. The sample was cut to the final electrode size of 50 cm^2 ($72 \times 72\ mm^2$).

Finally the MEA was prepared in a hot pressing procedure using a hydraulic press (ENERPAC Düsseldorf, Germany, 25 kN, 125 °C, 6 min). The MEA consists of the self-made anode, a commercial cathode type ELE 0070 (Johnson Matthey, London UK) and a Nafion™ 212 membrane.

2.9. Electrochemical preparation of Pt catalysts

The electrochemical route is a three step procedure: firstly, the GDS was coated with the graphene ink, containing the ionomer, secondly, the dried layer was impregnated with a solution of the precursor salt H_2PtCl_6, followed by the electrochemical reduction. A detailed description of this procedure can be found in Ref. [33].

2.9.1. Preparation of the precursor layer

Different types of GDS were coated with dispersions containing:

(i) Pure graphene,
(ii) Graphene/carbon black mixtures and
(iii) Graphene/MWCNT mixtures.

For graphene/carbon black mixtures, a $10 \times 20\ cm^2$ GDS was coated in a doctor blade process with an ink containing 375 mg graphene/carbon black, 1 mL H_2O, 1.28 mL isopropanol, 1.785 mL Nafion™ solution (20 wt.%). For homogenization ultrasound was applied for 10 min.

The prepared layers were dried at 140 °C for 30 min. The precursor salt was dissolved in isopropanol. Thereafter the coated GDS was impregnated in a dip-coating process with the alcoholic precursor solution. After drying for 12 h in vacuum the working electrode is ready for the electrochemical reduction. The GDE was cut to the final size of 50 cm^2 ($72 \times 72\ mm^2$).

2.9.2. Electrodeposition

The pulsed electrodeposition was carried out in a fuel cell like setup using a SP150 potentiostat (Biologic, Grenoble, France) which is connected to a VMP3B-10 amplifier (10A/20V). A scheme is given in Fig. 1. The working electrode consists of a GDS coated with graphene or graphene/carbon black containing the platinum precursor and was purged with dry nitrogen ($100\ mL\ min^{-1}$). The commercial counter electrode (type ELE0171, $1.5\ mg\ Pt\ cm^{-2}$) was purchased from Johnson Matthey. A Nafion™ 115 membrane (DuPont) was used as proton exchanging electrolyte. The proton conductivity of the membrane was maintained by the use of humidified hydrogen ($40\ mL\ min^{-1}$, dew point 25 °C). The working electrode potential was set to 50 mV vs. DHE (dynamic hydrogen electrode) for 1 ms during the nucleation phase and to 150 mV vs. DHE for 100 ms during the growth phase. The working electrode was set to open circuit potential (OCP) for 50 ms in the pulse break; the total deposition time was 15 min. Starting from the so prepared GDE the full MEA was obtained according to the hot-pressing procedure given in Section 2.8.

For the characterization of the resulting samples, pieces of 1 cm^2 were cut out of the working electrode, which were ultrasonicated in isopropanol to dispense the Pt/C layer from the GDE. After evaporating the solvent the solid residue was chemically analyzed to determine the platinum content and structurally characterized to measure the catalyst size and the distribution.

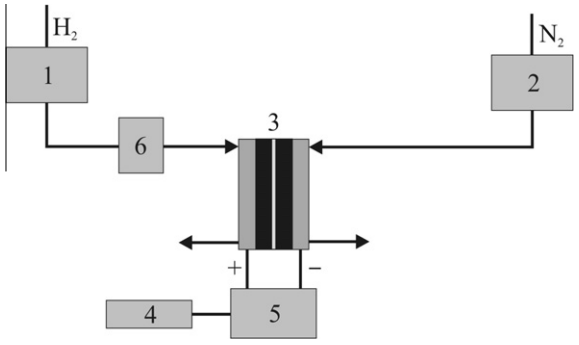

Fig. 1 – Experimental setup for the electrochemical catalyst reduction (1, 2: mass flow controllers for H_2 and N_2, 3: deposition cell, 4: potentiostat, 5: amplifier, 6: humidification).

2.10. Polarization measurements on MEAs

All the experiments were carried out under standard pressure conditions. The current-voltage curves of single-cell fuel cells were recorded using a modular test bench. The reactant stoichiometry was kept constant at $\lambda = 1.2$ or $\lambda = 1.5$ for hydrogen and $\lambda = 2.0$ or $\lambda = 2.5$ for oxygen. The hydrogen (grade: 5.0) and the oxygen (grade: 4.5) were humidified. For the MEA characterization, a 50 cm^2 fuel cell housing was used. The setup for humidification of the gases consisted of a boiling water reservoir, a condensing unit (MC-tech, Germany) and heated tubes (Horst, Germany), connected to the fuel cell. The condenser devices were kept at a constant temperature using thermostats; the temperature of the heated tubes was preferably 5 °C higher than the corresponding dew point (T_{dew}; dp_a – dew point anode and dp_c – dew point cathode) to exclude condensation inside the tubes. The relative humidity (RH) can be calculated for given T_{dew} and T_{Cell} values. A dew point mirror (Michell, Bad Homburg, Germany) was used to control steam-related parameters like RH and T_{dew}. The highest realizable T_{dew} was 80 °C and was related to the specific humidification principle. The RH was kept constant during the measurements, preferably at 95%, on the anode and cathode side. A galvanostatic operation mode was used for all polarization experiments; typical current increase steps were in-between 2–5 A and the corresponding time steps were in the range of 300–600 s. The samples and the experimental parameters are summarized in Table 2.

Quasi-stationary current-voltage curves were reached after 4–5 cycles for a given set of operational parameters (Table 2), corresponding to an operation time of at least 10 h. The experiments were carried out in hydrogen/oxygen mode at 60 and 80 °C.

3. Results and discussion

3.1. Macrostructures of different graphene types

Fig. 2A and B show electron microscopic images of AO-2 graphene. The graphene flakes are well separated and consist of 44-52 monolayers, which can be clearly seen in the TEM image (Fig. 2B). The thickness of the multilayer flakes is between 11 and 13 nm.

Fig. 2C shows also well-dispersed graphene flakes of sample C1, which tend to exhibit a very rough surface structure. The average multilayer flake thickness is 3.7–4.0 nm (Fig. 2D), corresponding to 15–32 monolayers. As can be seen in the SEM pictures, the flakes built up a good connected network which is crucial for the electron transport in electrocatalytic applications.

3.2. Microstructure of the graphene supports

The Raman spectra of different graphene samples are shown in Fig. 3. The spectra of AO-2, AO-2/Pt, and C1 samples look very similar with no significant differences. There are mainly three typical lines observable: the so-called D-line, G-line, and the D*-line. The D-line and the G-line are due to first order Raman scattering. The D*-line (in literature also sometimes called 2D or G′) is due to second order Raman scattering.

The appearance of the relatively weak D-line is associated with disorder and edge effects in graphitic samples [38]. Such spectra are commonly observed in Raman measurements performed on graphite [39]. This observation is not unexpected because the layer thicknesses of the flakes range from 5 to 13 nm. At this thickness the flakes consist of $\geqslant$10 monolayers of graphene. Ferrari et al. showed that the spectra for more than 5–10 monolayers of graphene look very similar to spectra measured on graphite [40].

3.3. Structure of the catalyst support layer

Catalyst support layers were prepared according to the method described in Section 2.8 and 2.9. The structure was analysed by AFM. It can be clearly seen in Fig. 4 that the graphene flakes form a very dense roof tile structure. It results from a slow segregation process during the evaporation of the solvent. This result has the consequence that a fuel cell MEA prepared with this material is expected to have a very poor performance under real operating conditions because this structure causes a strong mass transport limitation for fuels and products.

A solution for this problem could be the placement of spacers between the graphene flakes. Carbon black particles, multi-walled nanotubes or both together could generate the necessary porous structure. According to this concept, a sample consisting of a mixture of graphene flakes and multi-walled carbon nanotubes was prepared. The AO-2 graphene/MWCNT-ratio was 2:1 (wt.%). As can be seen in Fig. 5A the graphene flakes and the MWCNT additives form a homogeneous mixture in which the MWCNT additives are located between the graphene flakes. The mixtures of graphene flakes

Table 2 – Test bench parameters for MEA characterization.

No.	Reduction method*	Anode	dp_a (°C)	dp_c (°C)	λ_{O_2}	λ_{H_2}	T_{cell} (°C)
1	CCR	0.30 mg cm−2 Pt; pure AO-2	59	59	2.0	1.2	60
2	ECR	0.20 mg cm^{-2} Pt; AO-2/carbon black 1:1	79	79	2.0	1.2	80
3	CCR	0.16 mg cm^{-2} Pt; AO-2/MWCNT 2:1	72	78	2.0	1.5	80
4	CCR	0.25 mg cm^{-2} Pt; AO-2/carbon black 1:1	80	80	2.0	1.2	80
5	Reference	0.40 mg cm^{-2} Pt (ELE0162)	80	80	2.0	1.2	80
6	CCR	0.16 mg cm^{-2} Pt; AO-2/carbon black 1:2	72	78	2.5	1.5	80
7	CCR	0.19 mg cm^{-2} Pt; AO-2/carbon black 2:1	72	78	2.5	1.5	80
8	ECR	0.20 mg cm^{-2} Pt; pure AO-2	59	59	2.0	1.2	60

* CCR: chemical catalyst reduction, ECR: electrochemical catalyst reduction.

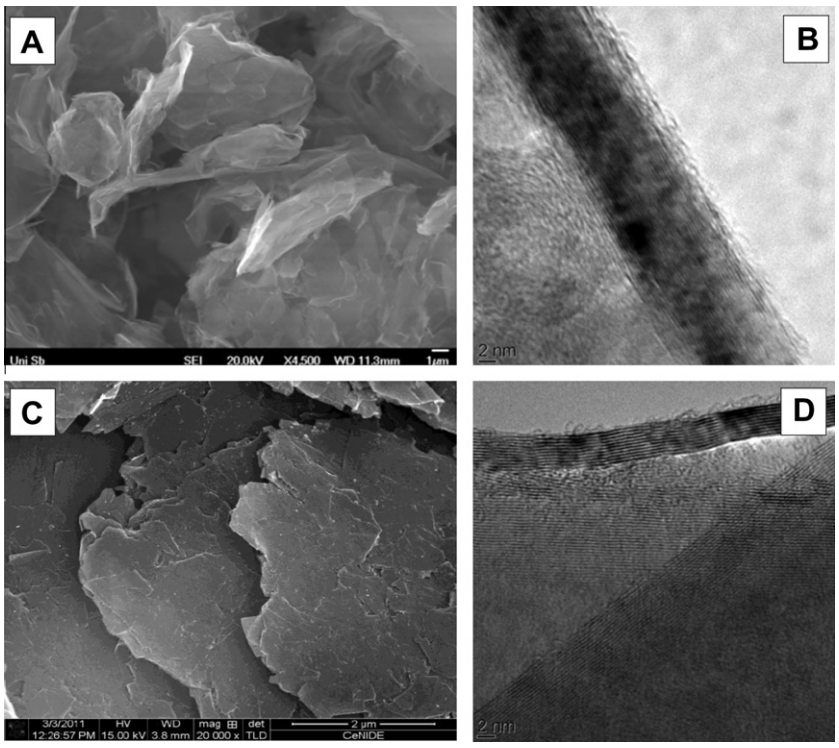

Fig. 2 – SEM images of graphene AO-2 (A) and C1 (C) and TEM images of AO-2 (B) and C1 (D).

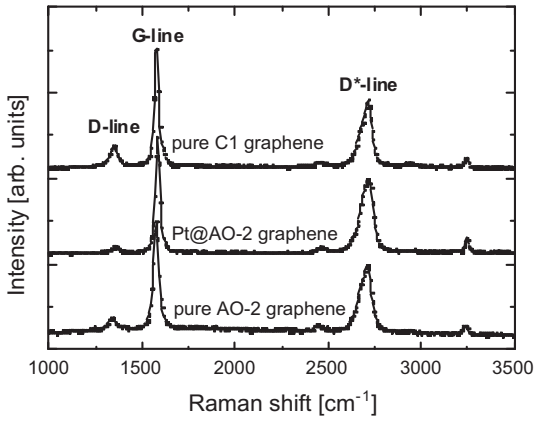

Fig. 3 – Raman spectra of different graphene types and a Pt/graphene sample.

and large carbon black particles (Cancarb) were prepared in a similar way. The AO-2 graphene:carbon black ratio was 1:1 (wt.%). The carbon black particles (Fig. 5B) with a diameter of 200–500 nm are also well distributed between the graphene flakes and act as spacers.

3.4. *Catalyst preparation*

Numerous methods for the preparation of fuel cell catalysts are reported in the literature. All these methods can be divided into two groups. The first group is the chemical or thermal reduction of platinum precursors with simultaneous immobilisation on a carbon support which were afterwards appliqued on a GDS. The second group involves electrochemical methods which are able to reduce platinum precursors directly at the triple-phase regions in a half or full MEA. The influence of the preparation method on the fuel cell performance was measured on catalysts prepared with both methods.

3.4.1. *Chemical route*

It is well known that chemical impurities lead to a deactivation of fuel cell catalysts. For this reason it is necessary to analyze the purity of the used materials. Significant impurities are listed in Table 3. For the used materials the type and amount of the detected elements are not critical for the present experiments.

For all preparation methods the platinum precursor (H_2PtCl_6) must adsorb on the surface of the carbon support. Therefore the graphene surface should have a negative surface potential. In Zeta-Potential measurements a surface potential of −49 mV and −37.6 mV was determined for AO-2 and C1, respectively. This negative Zeta potential was also observed in the literature for chemically converted graphene [41].

The preparation method is described in Section 2.8. The as-prepared Pt/graphene samples with a platinum loading of 19 wt.% (Fig. 6A and B) show a homogenous distribution of the catalyst particles with a relatively small particle size (3–5 nm). Only a few agglomerates with a diameter of 30–60 nm can be observed. Fig. 6C and D show TEM pictures of a sample with a higher Pt loading (54 wt.%), which shows bigger primary particles (6–10 nm) and larger agglomerates (40–70 nm).

Fig. 6E and F show the TEM pictures of the AO-2/MWCNT (2:1) supported platinum, where the catalyst particles are bonded onto the graphene flakes (Fig. 6E) and also to the

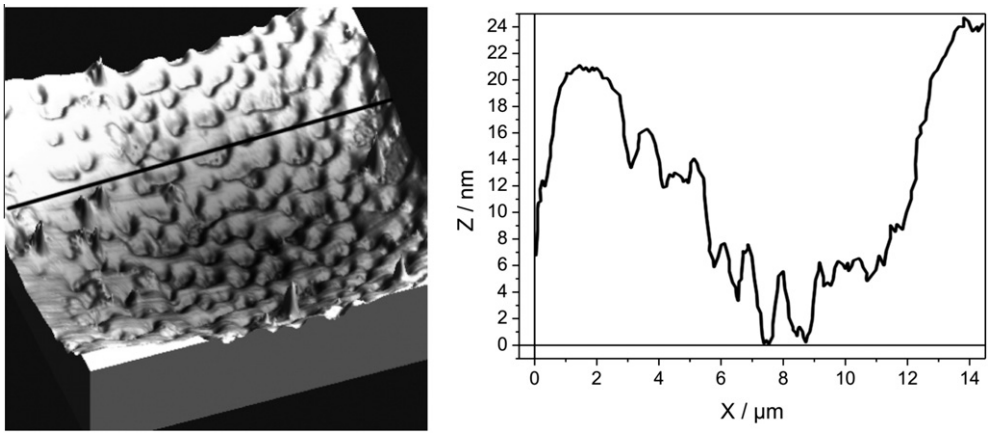

Fig. 4 – AFM measurement of the AO-2 graphene dispersed in N-methyl-pyrrolidone applied on a silicon wafer (measured area 15 × 15 µm²): 3 D picture of the sample (left) and height profile in the vertical direction (right). The line scan follows the black line in the left picture.

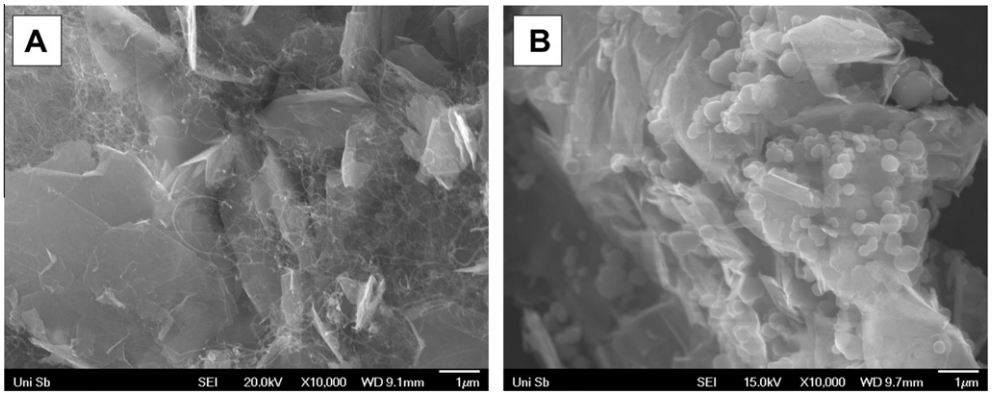

Fig. 5 – SEM picture (A) of the graphene/MWCNT (AO-2/MWCNT 2:1) and (B) of the AO-2/Cancarb carbon black (AO-2/Cancarb 1:1) system.

MWCNT additives (Fig. 6F). The particle size is in the range of 2–5 nm but some larger agglomerates (20–40 nm) can be observed.

Fig. 7A shows an overview of a Pt/AO-2/carbon black (1:1) supported catalyst sample. The carbon black particles are homogeneously distributed between the graphene flakes. A higher resoluted SEM image of this sample (Fig. 7B) shows that the catalyst deposition takes place on the graphene surface as well as on the carbon black particles.

The microstructure of the platinum catalyst was measured by X-ray diffraction (XPert-Diffractometer, PANalytical, Kassel, Germany).

Pure Cancarb carbon black, pure AO-2 graphene and also an AO-2/Cancarb carbon black (1:1) with thermally-reduced platinum catalysts were analyzed.

The results are shown in Fig. 8. The X-ray patterns of the AO-2 containing samples show a graphitic structure which can be identified with the JCPDS standard 75-2078. In contrast to the graphene samples, the pure Cancarb carbon black shows an amorphous structure without any peaks. The AO-2/Cancarb carbon black (1:1) sample with platinum shows the characteristic graphene peaks and the platinum diffraction pattern (JCPDS-file 04-0802). From the widths of the [220]-Bragg reflection a crystallite size of 4 ± 2 nm can be estimated according to Scherrer's law [44]. This particle size corresponds to the primary particle size detected from TEM images.

3.4.2. *Electrochemical route*

The potentiostatic electrodeposition method with the HDA, as well as catalyst supports such as graphene, graphene–carbon

Table 3 – Impurities of the graphene samples determined by ICP-OES.

Sample	O	Al	B	Ca	Fe	K	Mg
AO-2	<1.5%*	0.287%	0.236%	0.577%	0.194%	0.247%	0.117%
C1	<1.5%*	udl	udl	udl	udl	udl	udl

* Values determined by the manufacturer, udl: under detection limit.

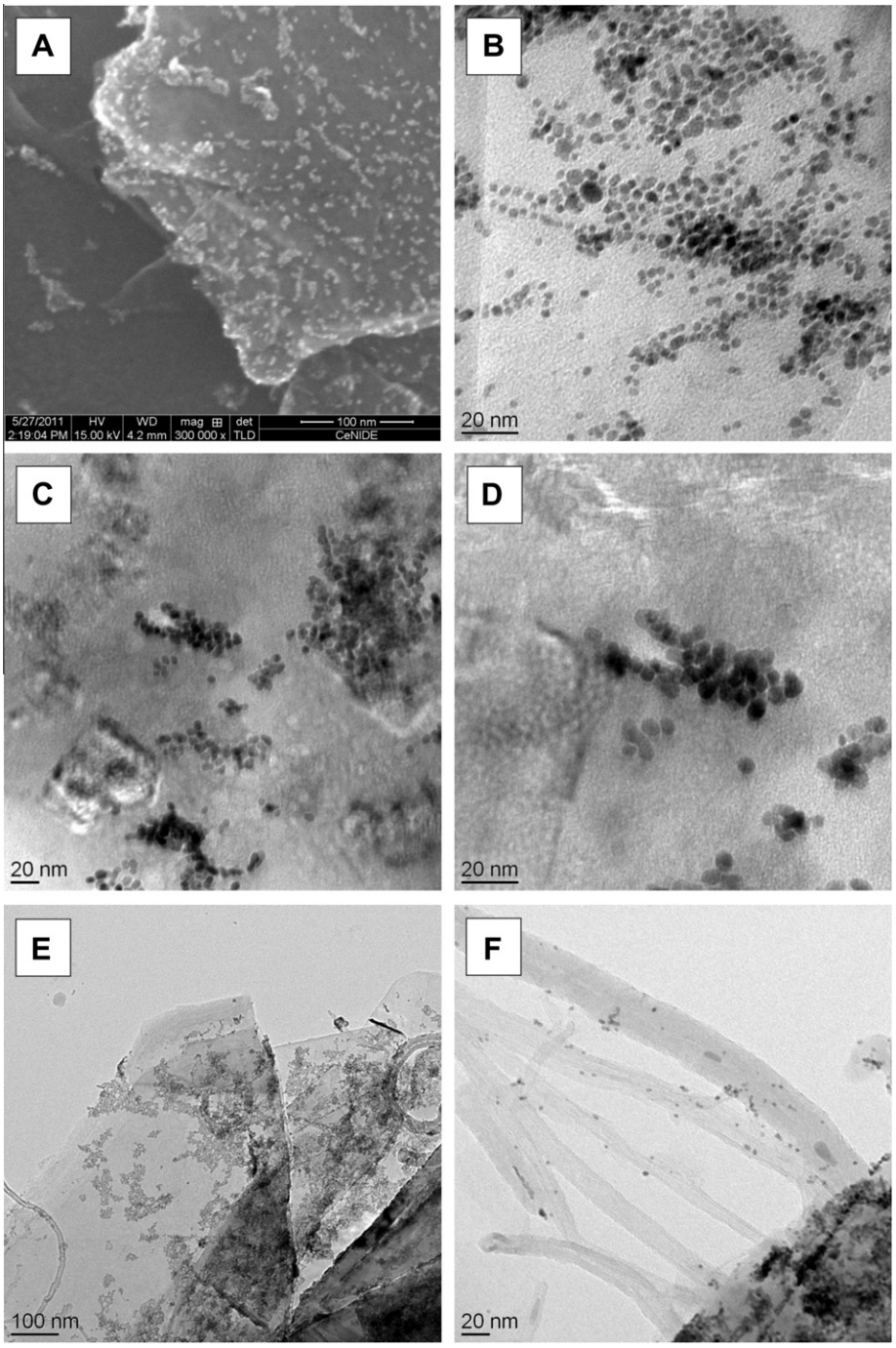

Fig. 6 – SEM picture (A) and TEM picture (B) of the chemically-reduced Pt (19 wt.%) catalysts on pure AO-2 graphene; TEM pictures (C and D) of chemically-reduced Pt (54 wt.%) catalysts on pure AO-2 graphene; TEM pictures (E and F) of Pt catalysts deposited on an AO-2 graphene/MWCNT mixture (2:1).

black or graphene/MWCNT mixtures were tested in this work. The electrochemical deposition method with the HDA has the advantage that it enables a precise control of the catalyst loading which leads to a very good distribution of the platinum particles on the supporting material. The electrochemical reduction method produces nearly quantitative platinum catalysts which are located at the TPBs which assures contact to the ionomer, the electron conducting phase and also to the fuel gases. In contrast to this method chemically-prepared catalysts have a fraction of up to 30% of inactive platinum particles.

The electrochemically-reduced catalysts show a slight agglomeration of the particles. The formation of agglomerates could result from the ingress of moisture during the electrodeposition process. The moisture enables migration of the very hygroscopic hexachloroplatinic acid which leads to small drops. During the electrochemical reduction the agglomerates were formed in these drops. The cell was flushed with dry n-

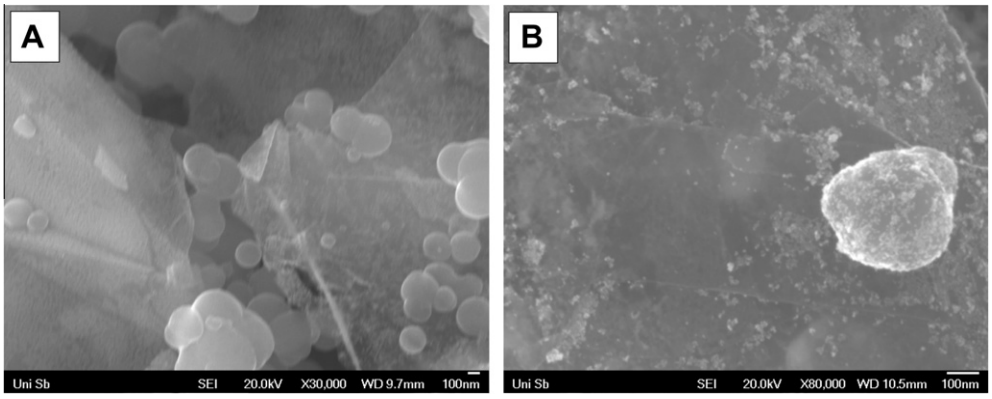

Fig. 7 – SEM pictures of chemically reduced Pt on an AO-2 graphene/Cancarb carbon black mixture (1:1).

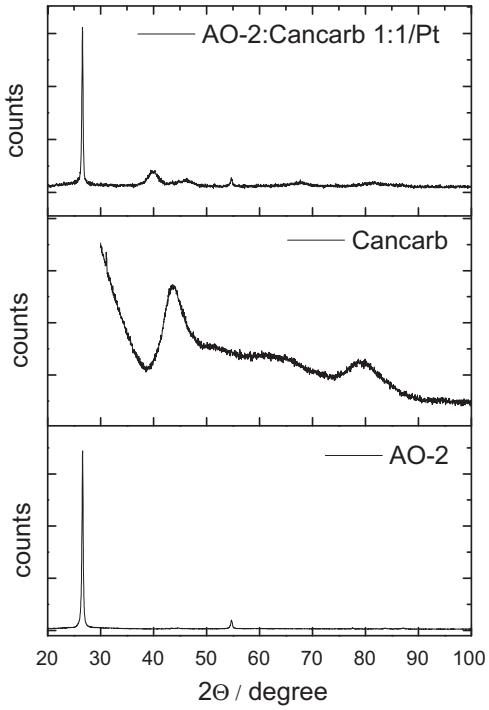

Fig. 8 – X-ray diffractograms of pure AO-2 graphene, Cancarb carbon black particles and a sample with AO-2/Cancarb 1:1 with platinum catalysts.

hexane to avoid the ingress of moisture, but some leaks cannot be avoided in the present setup. However, the efficiency of the method has been demonstrated in the present measurements. Fig. 9 (sample 2 and 8) shows the efficiency of an electrochemically-prepared catalyst. The performance of sample 2 is nearly the same as of a chemically-reduced catalyst but the electrochemically-reduced samples have a lower catalyst loading.

3.5. *Polarization measurements on MEAs*

Fig. 9A shows the polarization curves of MEAs consisting of gas diffusion anodes coated with different carbon supports and catalysts. The corresponding power densities are given in Fig. 9B. Fig. 10 is a comparison of all measured MEA-performances determined at a voltage of 650 mV.

Gas diffusion anodes coated with pure graphene as a supportive material show strong mass transport limitations and therefore a very low performance (sample 1) was observed. The addition of carbon black particles (sample 2, 4, 6, 7) or MWCNT (sample 3) additives reduces the mass transport problems and therefore higher power densities were received. Compared to sample 1 (pure graphene, platinum loading 0.3 mg cm^{-2}), sample 4 shows a higher power density due to lower mass transport limitations. Even by reducing the platinum loading of the anode by 37.5% (0.25 mg cm^{-2}) sample 4 showed a comparable performance to a commercial state-of-the-art reference with a platinum loading of 0.4 mg cm^{-2} on the anode.

In the case of gas diffusion anodes prepared with electrochemically reduced catalysts (sample 2, 8) similar results were received but the performance at higher current densities is not as good as the performance of the reference sample. The anodic platinum loading of samples 2 and 8 is lower (0.2 mg cm^{-2}) than the loading of the reference sample (0.4 mg cm^{-2}). As expected an anode prepared with pure graphene supported catalysts (sample 8) shows a very low performance.

The best results were obtained with chemically reduced catalysts (sample 4) with a catalyst loading of 0.25 mg cm^{-2}. Sample 2 with a catalyst loading of 0.2 mg cm^{-2} has a power density of 0.63 W cm^{-2} at 650 mV. It is in the range of the power density of sample 1 (pure graphene) which has a higher catalyst loading of 0.3 mg cm^{-2}.

These results confirm our hypothesis that the addition of carbon black, MWCNT or other conductive additives to the graphene matrix leads to a porous network structure which reduces the mass transport limitations.

3.6. *Ohmic resistance measurements*

The area specific electric resistance of the uncoated GDS decreased from 29 mΩ cm^2 at 2.5 bar to 18 mΩ cm^2 at 30 bar (Fig. 11A). The sample with the Vulcan/Nafion™ layer shows a similar behavior to the uncoated GDS but the area specific resistance is slightly higher. The curve of the coated layer is

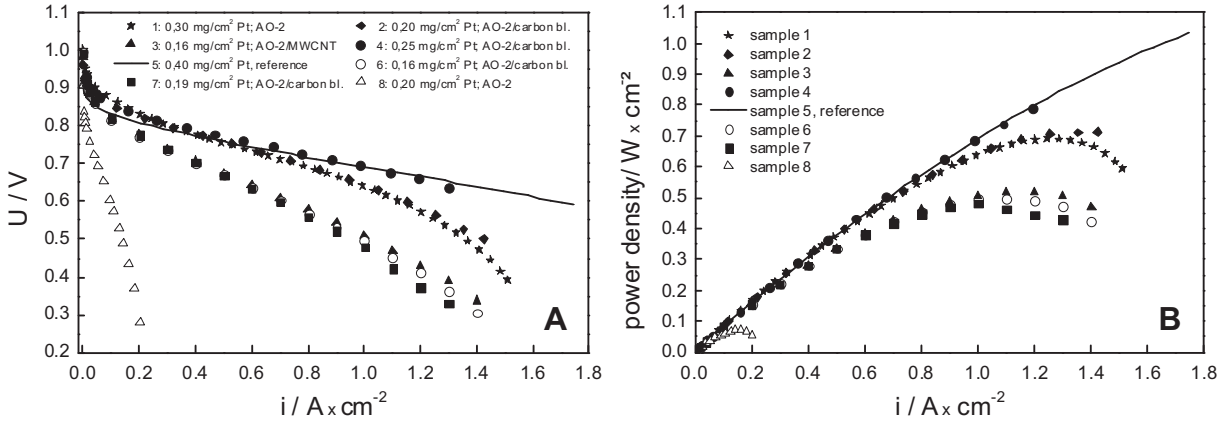

Fig. 9 – Polarization curves of the measured MEAs (A) and corresponding power densities (B); detailed sample composition is given in Table 2.

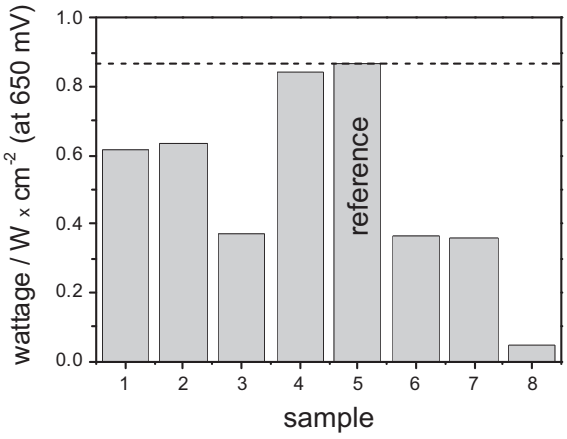

Fig. 10 – Performances of the MEAs measured at 650 mV. Sample 5 is a reference sample made of a commercial cathode and anode (the platinum loading is 0.4 mg cm^{-2}).

shifted by 1 mΩ cm^2 to higher area specific resistances which can be explained with the extra transition resistance resulting from the Vulcan/Nafion™ layer.

The area specific resistance decreases from 26 mΩ cm^2 at 2.5 bar to 17 mΩ cm^2 at 30 bar and shows within the range of measurement error the same values as the uncoated GDS sample. From these experiments it can be concluded that the area specific resistance of a gas diffusion electrode is mainly influenced by the GDS material and is not significantly changed by a 10 μm thick graphene/Nafion™ layer.

There is a qualitative correlation between cell resistances and the measured power densities of the MEAs (Fig. 11B). The anodic catalyst support of sample 6 (0.16 mg cm^{-2} Pt on AO-2/carbon black 1:2) and 7 (0.19 mg cm^{-2} Pt on AO-2/carbon black 2:1) consists of a graphene/carbon black mixture. Sample 3 was prepared with a mixture of AO-2/MWCNT 2:1 (catalyst loading 0.16 mg cm^{-2} Pt). Compared to sample 3, the graphene/carbon black mixtures (samples 6 and 7) show a slightly lower wattage and a higher ohmic resistance. There are significant differences between the cell resistances which correlate to the polarization curves. The difference in the resistance between sample 3 and 7 is about 1 mΩ, which is a really high value. For 50 cm^2 it corresponds to an area specific resistance of 50 mΩ cm^2. At 1 A cm^{-2} we observe a difference in the voltage of 30 mV and at 1.2 A cm^{-2} a difference of 58 mV. Sample 3 (graphene/MWCNT) shows the highest power density and the lowest ohmic resistance. These results indicate that the addition of MWCNT additives leads to a more efficient conductive network between the graphene flakes as demonstrated in Fig. 11B. Comparing sample 6 (graphene/carbon black 1:2) and 7 (graphene/carbon black 2:1), we observe a lower ohmic resistance for sample 6. The higher carbon black content of sample 6 causes a better percolation between the graphene flakes and the carbon black particles form a conductive network. The increased number of contact points between the carbon structures might be responsible for the higher electronic conductivity due to decreased resistance.

4. Conclusion

Different graphene types were tested for electrochemical energy conversion especially for fuel cell applications. It could be shown that pure graphene forms a very dense and ordered structure during the coating process of gas diffusion layers. For this reason the produced MEAs suffered from a very low performance. Carbon black and MWCNT were used to act as spacers between the graphene flakes, in order to increase the exposed surface area of the graphene, the electronic conductivity and the mass transport of the reactants and products. The porous structure of the graphene/MWCNT-supported Pt or graphene/carbon black supported Pt provides a fast diffusion of fuels and products to and from the active sites, avoiding mass transport limitations. The carbon spacers have a bifunctional role in this system. Firstly, the structure provides a good spacer for reactant and product diffusion, and secondly, they build a huge electronic contact network. There is a qualitative correlation between the changes of the cell resistances and the measured power density of the MEAs. For this reason a combination of graphene/fiber-like or graphene/particle-like carbon structures seems to be a very good catalyst support for fuel cell applications. The present experiments show that the over-all efficiencies of commercially fuel cell systems can be achieved with 37% less noble

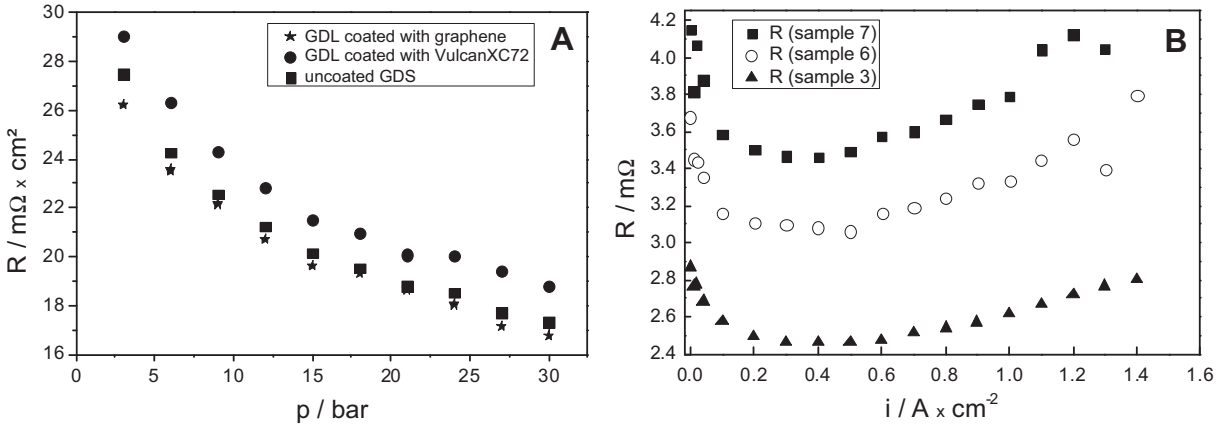

Fig. 11 – (A) Pressure-dependent through-plane resistances of an H2315 I3C4-GDS, an H2315 I3C4-GDS coated with Vulcan XC72R/Nafion™ and H2315 I3C4-GDS coated with AO2-graphene/Nafion™; (B) In situ cell resistance measurements for MEAs prepared with graphene/carbon black mixtures (sample 6 and 7) and with graphene/MWCNT (sample 3).

metal. The cost calculation for a complete fuel cell system based on this technique is difficult because currently the graphene materials were produced only in a small scale (mostly for scientific research) and are relatively expensive (20 US-$/g). In the case of a large scale production of these materials the price will decrease strongly. A calculation with the actual platinum price (1465 US-$/oz) shows that the platinum costs for the commercial anode is 21 US-$/kW and 13 US-$/kW for our graphene based anode. Based on these results we await the production of much cheaper and more efficient fuel cells for the future. However, the application of graphene and graphene-based materials in the field of fuel cells is still in its infancy and many challenges remain. The development of well controlled methods for synthesis when processing graphene- or graphene composite-based catalysts is still under way and the first results are only beginning to emerge. Still more work and a better understanding of the correlation between the electrochemical performance and graphene structures, between the interactions of the graphene- and graphene composite-supported catalysts and their properties, is needed. Future work will include developing the most suitable methods and ways for preparing graphene- and graphene composite-based catalysts for fuel cell applications. This means also the reduction of the platinum loading by keeping the same good achievements, as well as searching for other methods, which enable the enhancement of the catalytic effect while further reducing the platinum loading, or even completely replacing the cost-effective metal catalysts in fuel cells by other efficient, low-cost and stable electrode materials. This “green route” could be a challenge and also a perspective for the next generation [45–49].

Acknowledgments

This work was financially supported by the Bundesministerium für Bildung und Forschung within the framework of the WING programme (Einsatz von Graphenen in der Energietechnik – Lithiumbatterien und Brennstoffzellen – LiBZ). We wish to thank Sylvia Kuhn, Tanja Müller, Elfi Jungblut, Dieter Münch, Dr. Haibin Gao, Christoph Thome, Sabrina Fricke, Franco Cappuccio and Andreas Witzmann. We also thank Prof. Dr. Rolf Hempelmann, Bernd Oberschachtsiek and Prof. Dr. Axel Lorke for stimulating and fruitful discussions.

REFERENCES

[1] Castro Neto AH, Guinea F, Peres NMR, Novoselov KS, Geim AK. The electronic properties of graphene. Rev Mod Phys 2009;81:109–62.
[2] Balandin AA, Ghosh S, Bao W, Calizo I, Teweldebrhan D, Miao F, et al. Superior thermal conductivity of single-layer graphene. Nano Lett 2008;8(3):902–7.
[3] Novoselov KS, Geim AK, Morozov SV, Jiang D, Zhang Y, Dubonos SV, et al. Electric field effect in atomically thin carbon films. Science 22 October 2004;306(5696):666–9.
[4] Geim AK, Novoselov KS. The rise of graphene. Nat Mater 2007;6:183–91.
[5] Katsnelson IM. Graphene: carbon in two dimensions. Mater Today 2007;10(1–2):20–7.
[6] Lee C, Wei1 X, Kysar WG, Hone J. Measurement of the elastic properties and intrinsic strength of monolayer graphene. Science 18 July 2008;321(5887):385–8.
[7] Guinea F, Katsnelson IM, Geim AK. Energy gaps and a zero-field quantum Hall effect in graphene by strain engineering. Nat Phys 2010;6:30–4.
[8] Stoller DM, Park S, Zhu Y, An J, Ruoff SR. Graphene-based ultracapacitors. Nano Lett 2008;8(10):3498–502.
[9] Dikin AD, Stankovich S, Zimney JE, Piner DR, Dommett HBG, Evmenenko G, et al. Preparation and characterization of graphene oxide paper. Nature 2007;448:457–60.
[10] Park H, Rowehl AJ, Kim KK, Bulovic V, Kong J, Park Hyesung, et al. Doped graphene electrodes for organic solar cells. Nanotechnology 2010;21(50):1–6.
[11] Reddy D, Register FL, Carpenter DG, Banerjee KS. Graphene field-effect transistors. J Phys D 2011;44:1–20.
[12] Bunch SJ, van der Zande MA, Verbridge SS, Frank WI, Tanenbaum , Parpia MJ, et al. Electromechanical resonators from graphene sheets. Science 2007;315(5811):490–3.
[13] Pumera M, Ambrosi A, Bonanni A, Khim Chng EL, Ling Poh H. Graphene for electrochemical sensing and biosensing. Trends Anal Chem 2010;29(9):954–65.
[14] Wang L, Lee K, Sun Y-Y, Lucking M, Chen Z, Zhao JJ, et al. Graphene oxide as an ideal substrate for hydrogen storage. ACS Nano 2009;3(10):2995–3000.

[15] Ji Q, Honma I, Paek S-M, Akada M, Hill PJ, Vinu A, et al. Layer-by-layer films of graphene and ionic liquids for highly selective gas sensing. Angew Chem Int Ed 2010;49:9737–9.
[16] Pumera M. Graphene in biosensing. Mater Today 2011;14:308–15.
[17] Xu Z, Tai G, Zhou Y, Gao F, Wong HK. Self-charged graphene battery harvests. Electricity from Thermal Energy of the Environment 2012. <http://arxiv.org/abs/1203.0161>.
[18] Liu Z, Robinson TJ, Tabakman MS, Yang K, Dai H. Carbon materials for drug delivery and cancer therapy. Mater Today 2011;14(7–8):316–23.
[19] Pant D, Singh A, Van Bogaert G, Alvarez-Gallego Y, Diels L, Vanbroekhoven K. An introduction to the life cycle assessment (LCA) of bioelectrochemical systems (BES) for sustainable energy and product generation: relevance and key aspects. Renew Sustain Energy Rev 2011;15(2):1305–13.
[20] Chaparro AM, Benitez R, Scherer GG, Daza L. Study of membrane electrode assemblies for PEMFC, with cathodes prepared by the electrospray method. J Power Sources 2007;169:77–84.
[21] Esmaeilifar A, Rowshanzamir S, Eikani MH, Ghazanfari E. Synthesis methods of low-Pt-loading electrocatalysts for proton exchange membrane fuel cell systems. Energy 2010;35:3941–57.
[22] Pant D, Van Bogaert G, De Smet M, Diels L, Vanbroekhoven K. Use of novel permeable membrane and air cathodes in acetate microbial fuel cell. Electrochim Acta 2010;55:7710–6.
[23] Zhang F, Pant D, Logan BE. Long-term performance of activated carbon air cathodes with different diffusion layer porosities in microbial fuel cells. Biosens Bioelectron 2011;30(1):49–55.
[24] Pant D, Van Bogaert G, Porto-Carrero C, Diels L, Vanbroekhoven K. Anode and cathode materials characterization for a microbial fuel cell in half cell configuration. Water Sci Technol 2011;63(10):2457–61.
[25] Alvarez-Gallego Y, Dominguez-Benetton X, Pant D, Diels L, Vanbroekhoven K, Genné I, et al. Development of gas diffusion electrodes for cogeneration of chemicals and electricity. Electrochim Acta 2012;82:415–26.
[26] Hou J, Shao Y, Ellis WM, Moore BR, Yi B. Graphene-based electrochemical energy conversion and storage: fuel cells, supercapacitors and lithium ion batteries. Phys Chem Chem Phys 2011;13:15384–402.
[27] Shao YY, Yin GP, Gao YZ. Understanding and approaches for the durability issues of Pt-based catalysts for PEM fuel cell. J Power Sources 2007;171(2):558–66.
[28] Zhang S, Shao YY, Yin G, Lin Y. Stabilization of platinum nanoparticle electrocatalysts for oxygen reduction using poly(diallyldimethylammonium chloride). J Mater Chem 2009;19:7995–8001.
[29] Xu C, Wang X, Zhu JW. Graphene-metal particle nanocomposites. J Phys Chem C 2008;112(50):19841–5.
[30] Sharma S et al. Rapid microwave synthesis of CO tolerant reduced graphene oxide-supported platinum electrocatalysts for oxidation of methanol. J Phys Chem C 2010;114(45):19459–66.
[31] Seger B, Kamat P. Electrocatalytically active graphene-platinum nanocomposites. Role of 2-D carbon support in PEM fuel cells. J Phys Chem C 2009;113:7990–5.
[32] Hou JB et al. Electrochemical impedance investigation of proton exchange membrane fuel cells experienced subzerotemperature. J Power Sources 2007;171(2):610–6.
[33] Mitzel J, Arena F, Natter H, Walter T, Batzer M, Stefener M, et al. Electrodeposition of PEM fuel cell catalysts by the use of a hydrogen depolarized anode. Int J Hydrogen Energy 2012;37:6261–7.
[34] Stankovich S, Dikin DA, Piner RD, Kohlhaas KA, Kleinhammes A, Jia Y, et al. Synthesis of graphene-based nanosheets via chemical reduction of exfoliated graphite oxide. Carbon 2007;45:1558–65.
[35] McAllister JM, Li J-L, Adamson HD, Schniepp CH, Abdala AA, Liu J, et al. Single sheet functionalized graphene by oxidation and thermal expansion of graphite. Chem Mater 2007;19:4396–404.
[36] Stankovich S, Piner RD, Chen XQ, Wu NQ, Nguyen ST, Ruoff RS. Stable aqueous dispersions of graphitic nanoplatelets via the reduction of exfoliated graphite oxide in the presence of poly (sodium 4-styrenesulfonate). J Mater Chem 2006;16:155–8.
[37] Niyogi S, Bekyarova E, Itkis ME, McWilliams JL, Hamon MA, Haddon RC. Solution properties of graphite and graphene. J Am Chem Soc 2006;128:7720–1.
[38] Pimenta MA, Dresselhaus G, Dresselhaus MS, Cançado LG, Jorio A, Saito R. Studying disorder in graphite-based systems by Raman spectroscopy. Phys Chem Chem Phys 2007;9:1276–90.
[39] Nemanich RJ, Solin SA. First- and second-order Raman scattering from finite-size crystals of graphite. Phys Rev B 1979;20:392–401.
[40] Ferrari AC, Meyer JC, Scardaci V, Casiraghi C, Lazzeri M, Mauri F, et al. Raman spectrum of graphene and graphene layers. Phys Rev Lett 2006;97:187401–4.
[41] Li D, Müller M, Gilje S, Kaner RB, Wallace GG. Processable aqueous dispersions of graphene nanosheets. Nat Nanotechnol 2008;3:101–5.
[42] Villar-Rodil S, Paredes JI, Martínez-Alonso A, Tascón JMD. Preparation of graphene dispersions and graphene–polymer composites in organic media. J Mater Chem 2009;19:3591–3.
[43] Paredes JI, Villar-Rodil S, Martínez-Alonso A, Tascón JMD. Graphene oxide dispersions in organic solvents. Langmuir 2008;24(19):10560–4.
[44] Scherrer P. Bestimmung der Größe und der inneren Struktur von Kolloidteilchen mittels Röntgenstrahlen. Göttinger Nachrichten 1918;2:98–100.
[45] Xiong W, Du F, Liu Y, Perez A, Supp JM, Ramakrishnan TS, et al. 3-D carbon nanotube structures used as high performance catalyst for oxygen reduction reaction. J Am Chem Soc 2010;132(45):15839–41.
[46] Gong K, Du F, Xia Z, Durstock M, Dai L. Nitrogen-doped carbon nanotube arrays with high electrocatalytic activity for oxygen reduction. Science 2009;23(5915):760–4.
[47] Wang S, Iyyamperumal E, Roy A, Xue Y, Yu D, Dai L. Vertically aligned BCN nanotubes as efficient metal-free electrocatalysts for the oxygen reduction reaction: a synergetic effect by co-doping with boron and nitrogen. Angew Chem Int Ed 2011;50(49):11756–60.
[48] Yun YS, Kim D, Tak Y, Jin H-J. Porous graphene/carbon nanotube composite cathode for proton exchange membrane fuel cell. Synth Met 2011;161:2460–5.
[49] Sharma S, Ganguly A, Papakonstantinou P, Miao XP, Li MX, Hutchison JL, et al. Rapid microwave synthesis of CO tolerant reduced graphene oxide-supported platinum electrocatalysts for oxidation of methanol. J Phys Chem C 2010;114:19459–66.